INTERNATIONAL JOURNAL OF REMOTE SENSING, 2017
http://dx.doi.org/10.1080/01431161.2017.1312623

Taylor & Francis
Taylor & Francis Group

Monitoring urban expansion using time series of night-time light data: a case study in Wuhan, China

Xin Xin[a,b], Bin Liu[a], Kaichang Di[a], Zhe Zhu[c], Zhongyuan Zhao[d], Jia Liu[a], Zongyu Yue[a] and Guo Zhang[e]

[a]State Key Laboratory of Remote Sensing Science, Institute of Remote Sensing and Digital Earth, Chinese Academy of Sciences, Beijing, China; [b]University of Chinese Academy of Sciences, Beijing, China; [c]Department of Geosciences, Texas Tech University, Lubbock, USA; [d]Department of Surveying and Mapping, Wuhan Resources and Planning Bureau, Wuhan, China; [e]State Key Laboratory of Information Engineering in Surveying, Mapping and Remote Sensing, Wuhan University, Wuhan, China

ABSTRACT

Real-time urban expansion information is important for understanding the socio-economic activities and construction policies in urban areas. Night-time light data, which are available at annual and monthly temporal resolutions, can facilitate better analysis of socio-economic activities. In this study, we proposed a novel calibration method for Defense Meteorological Satellite Program's Operational Line-scan System (DMSP/OLS) data based on Rational Function Model (RFM). Stable lit pixels were employed to validate the effectiveness of the proposed model. The deference of mean square error shows that RFM method is better than traditional quadratic polynomials method for 76% of the data sets. Urban areas from 1992 to 2013 were extracted based on the calibrated data. A correlation analysis and multiple linear regression analysis between socio-economic factors and DMSP/OLS data were performed for Wuhan, China. The results of correlation factors showed that the correlation coefficient between night-time lights and socio-economic factors was higher than 0.85. Population produced the highest correlation coefficient among all the socio-economic factors. Multiple linear regression analyses were also performed, and the results showed that population and urban area could enhance the R^2 in Wuhan, and population density could enhance the R^2 in a comparative city Ordos. The development driving forces of the city could be reflected in multiple linear regression analysis of the night-time light data and socio-economic factors. Moreover, we investigated the relationship between construction policy and urban expansion using the time-series night-time light data, and found that the night-time light data could also reflect the construction policy and monitor the urban expansion effectively.

ARTICLE HISTORY
Received 11 October 2016
Accepted 23 March 2017

1. Introduction

China has undergone rapid economic development and urbanization in recent decades. Urban area in China increased from 7438 km^2 in 1981 to 32,520.7 km^2 in 2005 (Liu et al.

CONTACT Bin Liu liubin@radi.ac.cn State Key Laboratory of Remote Sensing Science, Institute of Remote Sensing and Digital Earth, Chinese Academy of Sciences, Beijing, China

2012). Additionally, the population in China increased from 602 million in 1953 (First Population Census) to 1,370 million in 2010 (Sixth Population Census), an increase of 1.28 times. However, the censuses that have been carried out every 10 years, have limited the capability for updating urban expansion in real-time, which can be problematic for cities in China that are changing every day (Zhu et al. 2016).

High temporal frequency night-time light satellite data provide a possible solution. Night-time light data are indicator of human activity and urban lighting intensity (Amaral et al. 2005; Liu et al. 2012; Shi et al. 2014b; Sutton et al. 2001; Zhao, Zhou, and Samson 2015). Night-time light satellites can detect weak optical signals, and these signals are not affected by sunlight, shadows, vegetation, or other features on the Earth's surface. Global night-time light composites are available monthly or annually. They are useful for analysing urbanization and human activities in rapidly developing areas. There are two main sources of night-time light data: the Defense Meteorological Satellite Program's Operational Line-scan System (DMSP/OLS) (Elvidge et al. 1995, 1997; Johnson, Flament, and Bernstein 1994) and the Day/Night Band (DNB) on the National Polar-orbiting Partnership Visible Infrared Imaging Radiometer Suite (NPP/VIIRS) (Lee et al. 2006). The NPP/VIIRS data, which have a higher resolution and a wider spectrum detection range, are the upgraded version of DMSP/OLS data. The two satellites are both working at present. DMSP/OLS started working in 1973, and NPP/VIIRS was launched in 2009 (Elvidge et al. 2007). However, the earliest DMSP/OLS night-time light data that can be obtained are from 1992, and the earliest NPP/VIIRS data are available since April 2012 on the National Oceanic and Atmospheric Administration/National Geophysical Data Center (NOAA/NGDC) website (http://ngdc.noaa.gov/eog/dmsp/downloadV4composites.html). These night-time light data have been widely used in many areas, such as fire monitoring (Elvidge et al. 1995), gas flaring (Elvidge et al. 2009), urban area extraction (Imhoff et al. 1997; Shi et al. 2014a; Small, Pozzi, and Elvidge 2005; Zhang and Seto 2011), urban expansion monitoring (Liu et al. 2012; Zhou et al. 2014), socio-economic analysis (Amaral et al. 2005; Sutton et al. 2001), crisis monitoring (Li and Li 2014; Li et al. 2015), CO_2 emissions (Ou et al. 2015), and cloud detection (Xia et al. 2014). Asian cities have also gained much attention through the use of night-time light data (Ma et al. 2012; Shi et al. 2014b). Previous research has shown that DMSP/OLS data can be used to detect long time series of annual dynamic changes at a macro scale, and NPP/VIIRS night-time light data, which feature a higher spatial resolution, can provide better details of urban structure. There is a strong relation between urban development and urban construction policy in some cities of China (Li 2008), but few researchers have studied the correlation between them using night-time light data.

The long time series of night-time light data provide a great opportunity for monitoring urban expansion. However, due to the degradation of each DMSP/OLS satellite and the lack of on-board calibration, the satellites do not provide DMSP/OLS night-time light data with good comparability (Elvidge et al. 2009). Therefore, it is critical to calibrate the DMSP/OLS data before they can be used in long time-series analysis. Several researchers have used relative radiance calibration for DMSP/OLS data, and the most common method is calculating the correction factor using the quadratic regression model (Elvidge et al. 2009; Liu et al. 2012).

Calibrated night-time light data can be used to analyse the socio-economic activities. Correlation analysis is commonly used for this purpose (Amaral et al. 2005; Liu et al.

2012; Ma et al. 2012; Shi et al. 2014b), but this method is only effective for analysing the relation between a single factor and the night-time light data. There have been few studies using the multiple regression method to analyse night-time light data and many socio-economic factors altogether (Levin and Duke 2012). It is necessary to use the multiple regression method for a more detailed analysis between the socio-economic statistical data and the night-time light data, e.g. to reveal the relation between the night-time light data and different combinations of the socio-economic factors.

In this research, we performed a case study of urban expansion monitoring in Wuhan, China, using multi-scale time-series night-time light data in the following four steps. First, we developed a novel DMSP/OLS data calibration method based on the Rational Function Model (RFM), which had a better performance than the traditionally used quadratic polynomial model. We also proposed a new method to verify the calibration accuracy using stable lit pixels, which have a stable mapping relationship between two data sets. Second, we extracted the urban areas using DMSP/OLS data and analysed the expansion dynamics. Third, we investigated the correlations between the urban areas and the socio-economic data through correlation analysis and multiple linear regression analysis. Finally, we analysed the impacts of construction policy and human activity on urban expansion using both DMSP/OLS and NPP/VIIRS time-series data, respectively.

2. Data

Our study area is in Wuhan (30°33′N, 114°19′E, the capital city of Hubei Province), China (Figure 1), which is in the middle-lower Yangtze Plain. The Yangtze River flows across Wuhan and divides Wuhan into three towns: Wuchang, Hanyang, and Hankou. Wuhan is the core city of economic development in Wuhan city circle. Wuhan city circle is one of the city circles that are under national major urban planning and will become the fourth region in China after the Yangtze River Delta, Pearl River Delta, and Bohai Sea Economic Zone. It contains nine cities (Wuhan, Huangshi, Ezhou, Huanggang, Xiaogan, Xianning, Tianmen, Qianjiang, and Xiantao) with different levels of urban development.

Rapid growth of urban area, population, and gross domestic product (GDP) has occurred since the twentieth century. Until 2013, the urban area in Wuhan had reached 534.28 km^2, and the population had reached approximately 8 million, an increase of 20.1% from the population in 1992. Wuhan's GDP rose multiple times from 1992 to 2013 (the GDP in 1992 was 255.42 trillion Chinese Yuan and the GDP in 2013 was 10,069.48 trillion Chinese Yuan).

In this study, the cities in Wuhan city circle, which is an important part of the Yangtze Economic Zone in China, were selected for a comparative study.

Three categories of data, including night-time light data (DMSP/OLS data and DNB of NPP/VIIRS data), statistical data (GDP, urban area, electricity consumption, population, and population density), and administrative boundaries of the study area, were used in this study. The DMSP/OLS data were obtained from the NOAA/NGDC website. We chose the annual stable DMSP/OLS data in the Version 4 data set from 1992 to 2013, which were acquired by six DMSP satellites, including F10, F12, F14, F15, F16, and F18. A detailed list of the DMSP/OLS data we used is shown in Table 1. They all have 3000 km swath with a resolution of 30 arc-second geographic grids. The digital number (DN) values (ranging from 0 to 63 with 0 representing background value) represent the

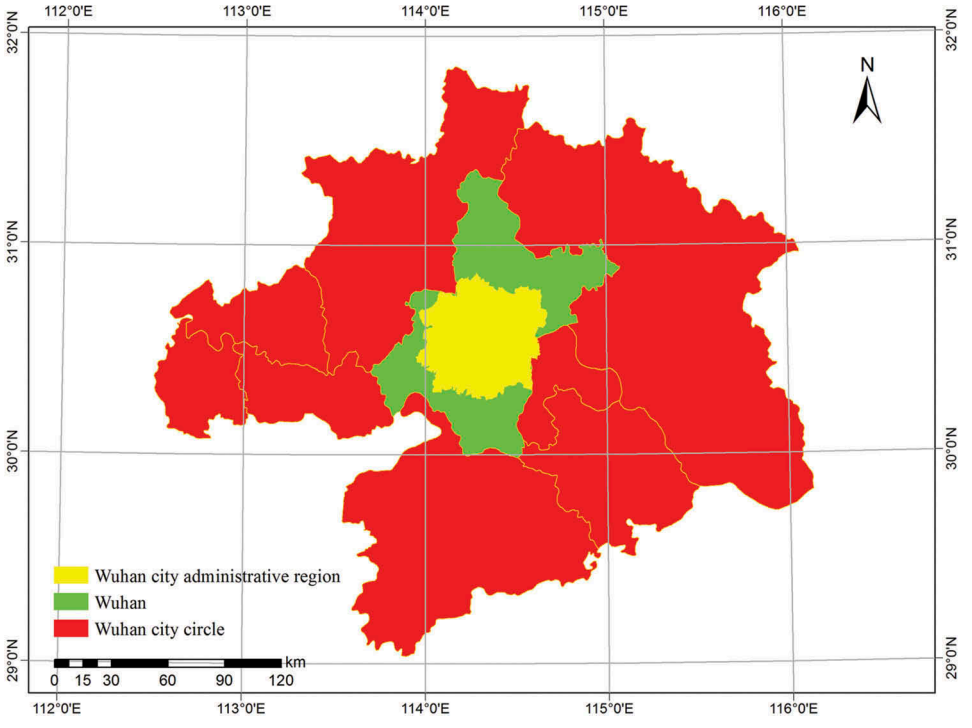

Figure 1. Study area.

Table 1. List of annual DMSP/OLS data.

Satellite Year	F10	F12	F14	F15	F16	F18
1992	F101992					
1993	F101993					
1994	F101994	F121994				
1995		F121995				
1996		F121996				
1997		F121997	F141997			
1998		F121998	F141998			
1999		F121999	F141999			
2000			F142000	F152000		
2001			F142001	F152001		
2002			F142002	F152002		
2003			F142003	F152003		
2004				F152004	F162004	
2005				F152005	F162005	
2006				F152006	F162006	
2007				F152007	F162007	
2008					F162008	
2009					F162009	
2010						F182010
2011						F182011
2012						F182012
2013						F182013

Table 2. The socio-economic statistics in Wuhan.

Year	GDP ($\times 10^9$ Chinese Yuan)	Urban area (km^2)	Electricity consumption ($\times 10^6$ kWh)	Population ($\times 10^4$)	Population density (people km^{-2})
1992	255.42	–	845669	684.46	–
1993	357.23	–	888289	691.69	–
1994	485.76	–	967882	700.01	827
1995	606.91	200.00	1011015	710.01	839
1996	782.13	202.00	1049970	715.94	846
1997	912.33	202.00	1086824	723.90	855
1998	1001.89	204.00	1079014	731.79	864
1999	1085.68	208.00	1024472	740.20	874
2000	1206.84	210.00	1186642	749.19	882
2001	1335.40	212.00	1524125	758.23	893
2002	1467.80	214.22	1587842	768.10	904
2003	1622.18	216.22	1788280	781.19	920
2004	1882.24	218.22	1855802	785.90	925
2005	2261.17	220.22	2108743	801.36	943
2006	2679.33	–	2308126	818.84	964
2007	3209.47	–	2586728	828.21	975
2008	4115.51	460.77	2864338	833.24	981
2009	4620.86	484.00	3102749	835.55	984
2010	5565.93	500.00	3536311	836.73	985
2011	6762.20	507.04	3836469	827.24	1180
2012	8003.82	520.30	4032605	821.71	1191
2013	9051.27	534.28	4372338	822.05	1203

average DN value of stable lights without filtering. The data were extracted according to the administrative boundaries of the study area and projected using the Mollweide projection (Snyder 1987), and then resampled to 1 km resolution.

The DNB data of NPP-VIIRS were also downloaded from the NOAA/NGDC website (http://ngdc.noaa.gov/eog/viirs/download_monthly.html). The monthly average radiance cloud-free composite images (January 2014, August 2014, December 2014, July 2015, and August 2015), which have undergone the stray-light correction procedure (Mills, Weiss, and Liang 2013), were chosen for this study. All the original data were in 15 arc-second geographic grids, and the data were resampled to the resolution of 500 m to facilitate analysis. The DN value of each pixel represents the radiation value of the pixel.

The socio-economic statistics used in this study were obtained from the Statistic Yearbook of Wuhan (Wuhan Bureau of Statistics 1992-2013). Table 2 shows the statistical data in details.

3. Methods

In our method, two types of night-time light data are used to monitor urban expansion and analyse correlations among night-time lights, socio-economic activities, and construction policy. Before the analysis, DMSP/OLS data need to be calibrated to improve their comparability. The relative radiance calibration of the DMSP/OLS data from 1992 to 2013 was based on RFM. Urban areas were extracted from the night-time light data after the calibration. Specially, urban areas were extracted from DMSP/OLS data based on the weighted light area, which is defined as the summing lit pixels multiplied by the normalized DN value (Ma et al. 2012). Areas were also extracted from NPP/VIIRS data through a thresholding method (Milesi et al. 2003).

As noted above, the DMSP/OLS data from the Version 4 data set cannot represent the real radiance value and cannot be used directly in long time-series urban analysis because of the lack of on-board calibration. DN values under the same light condition from different satellites are different. To address this problem, we developed a novel calibration method for DMSP/OLS data based on RFM. The new method involves two main steps: 1) inter-calibration of the annual data based on RFM, and 2) intra-annual composition and series correction of the inter-calibrated data. We also extracted stable lit pixels to verify the calibration method.

3.1. *Inter-calibration of the annual data*

The total number of lit pixels (Figure 2(a) and the average DN values (Figure 2(b)) were counted in each satellite year in China. It is obvious that the data are not directly comparable. There are large differences between different satellites in the same year. To improve the comparability of the time-series data, the data need to be inter-calibrated first. In this study, the reference satellite year was chosen as F162005, which has the minimum variance of the total lit pixel number and the average DN values between different satellites in the same year in Wuhan. In addition, by analysing the socio-economic characteristics of different cities in China, Jixi (a city in Heilongjiang Province), which has a wide spread of DN values and a stable state of socio-economic development, was selected as the reference calibration area (Liu et al. 2012). Inter-calibration was based on the aforementioned reference satellite year and reference calibration area. The most widely used inter-calibration method was developed by Elvidge et al. (2009) using a quadratic regression model. However, due to the characteristic of the quadratic regression curve, the points near the minimum/maximum DN values cannot fit well in some reference areas. RFM offers a good solution to this problem in our study. RFM, which can model functions with poles, is superior to polynomials models. An RFM is the quotient of two polynomials (Press et al. 2007). In this study, quadratic polynomial is used as the numerator and denominator of the RFM, which is given by the following equation:

$$D_C = \frac{p_1 \times D^2 + p_2 \times D + p_3}{D^2 + q_1 \times D + q_2}, \tag{1}$$

where

D_C is the inter-calibrated DN value of the data;
D is the original DN value of the source satellite year data; and
p_1, p_2, p_3, q_1 and q_2 are the coefficients of the second-order RFM;

The objective of this step is to inter-calibrate the lit pixels in each satellite year so that they are more comparable in time-series analysis. It is worth noting that the dark pixels, whose DN values are 0, are not involved in the inter-calibration.

3.2. *Intra-annual composition and series correction of the inter-calibration data*

The purpose of intra-annual composition is to make full use of the information derived from the data acquired in the same year from different satellites and remove the unstable lit pixels (Liu et al. 2012). Series correction is based on the assumption that

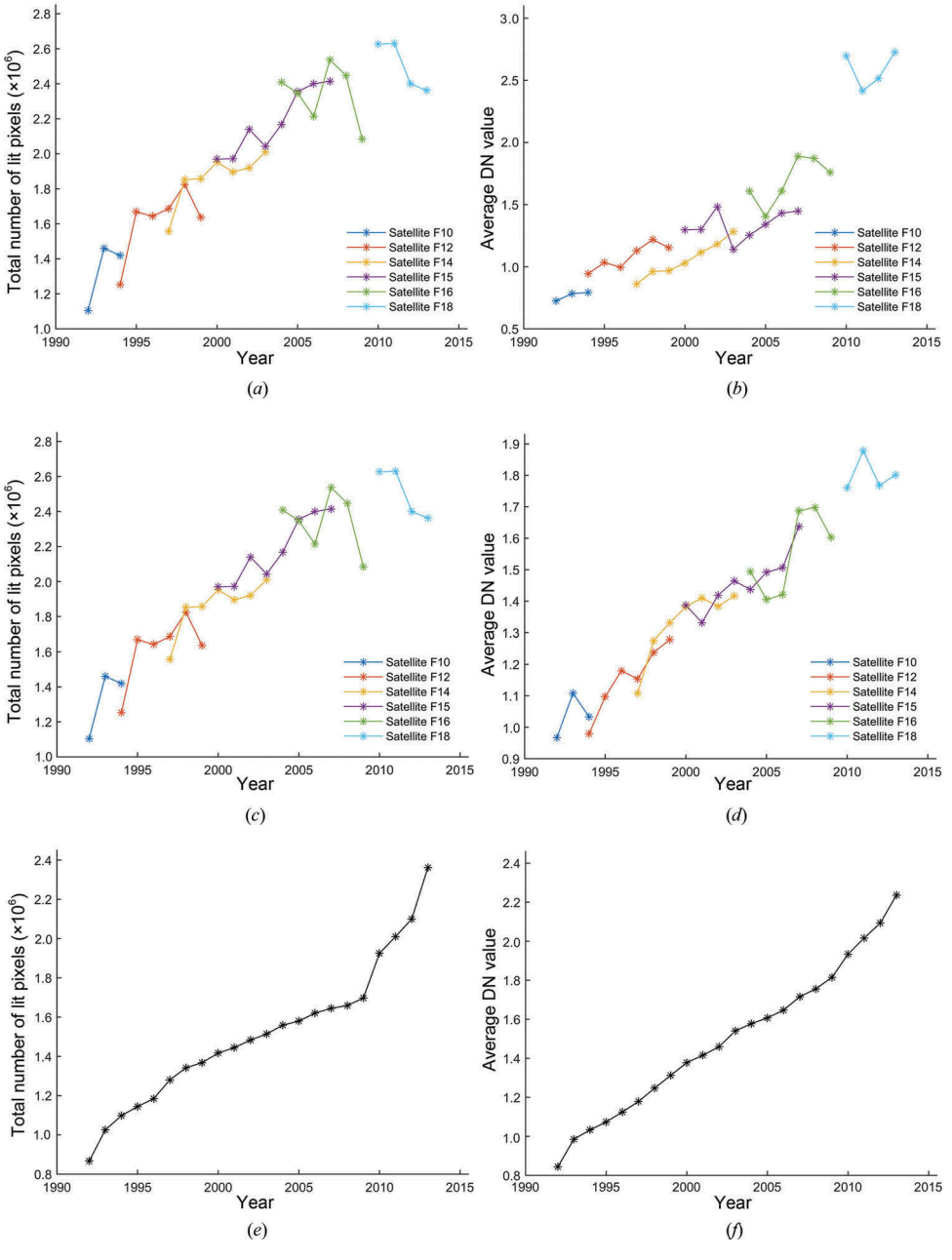

Figure 2. Total number of lit pixels (*a,c,e*) and average DN values (*b,d,f*) with respect to satellite year in China. (*a*) and (*b*) show the data before calibration. (*c*) and (*d*) show the data after inter-calibration. (*e*) and (*f*) show the data after both inter-calibration and intra-annual composition.

the urban area would grow continuously outwards and the lit pixels would become brighter over time (Liu et al. 2012).

Twelve composites acquired from two different satellites in the same year, containing the data set from 1994 and the data sets from 1997 to 2007, were intra-calibrated in this

study. The intra-annual composition results were the average values of the corresponding pixels in each data set that have different DN values from the two satellites:

$$D_n = (D_{n_1} + D_{n_2})/2, \tag{2}$$

where

D_n is the DN value of the data in the nth year after intra-annual composition; and

D_{n_1} and D_{n_2} are the DN values acquired in the nth year from satellites 1 and 2, respectively.

The intra-annual composition equation is applicable to the year n = 1994, 1997, 1998...,2007. For the other years in which there is only one satellite data available, $D_n$remains unchanged.

After intra-annual composition, series correction of the data was performed by the following equation (Liu et al. 2012):

$$D_{(n,i)} = \begin{cases} 0 & D_{(n+1,i)} = 0 \\ D_{(n-1,i)} & D_{(n+1,i)} > 0\ D_{(n-1,i)} > D_{(n,i)} \\ D_{(n,i)} & \text{otherwise} \end{cases}, \tag{3}$$

where

$D_{(n,i)}, D_{(n-1,i)}$ and $D_{(n+1,i)}$ are the DN values of the i th pixel in the nth, $(n-1)$th, and $(n+1)$th year, respectively. In the series correction, the data of the first year remained unchanged, whereas all the data of other years were processed using the above equation.

3.3. *Stable lit pixel extraction*

The calibration procedure aims to make the different DN values under the same night-time light condition as close as possible. To evaluate the effectiveness of RFM-based data calibration, we developed a method for generating stable lit pixels, whose DN value mapping relationship is less influenced by noises and real light condition changes.

Owing to the differences of measurement equipment and procedure, the DN values from different satellites under the same night-time light condition (acquired at the same position and the same time) may not be the same. The general forms of the mapping functions from the reference image to the calibrated images and from the calibrated images to the reference image can be represented by the following equations, respectively:

$$D_{\mathrm{R}} = F_{(n,\mathrm{R})}(D_n) + \delta_{(n,\mathrm{R})}, \tag{4}$$

$$D_n = F_{(\mathrm{R},n)}(D_{\mathrm{R}}) + \delta_{(\mathrm{R},n)},$$

where

D_{R} is the DN value of the reference image,

D_n is the DN value of the calibrated image in the nth year,

$\mathrm{F}_{(n,\mathrm{R})}$ and $\mathrm{F}_{(\mathrm{R},n)}$ are the mapping functions from the calibrated image to the reference image and the mapping function from the reference image to the calibrated image, respectively, and

$\delta_{(n,\mathrm{R})}$ and $\delta_{(\mathrm{R},n)}$ are the noise or error existing in the relationship.

By counting the DN value correspondences of the pixels at the same position between the reference image and the calibrated image, we considered the maximum correspondence numbers of all the DN values (1–62) as the candidates. The candidate sets are named as $O_{(n,R)}$ and $O_{(R,n)}$, respectively. We defined the pixels that exist both in set $O_{(n,R)}$ and in set $O_{(R,n)}$ as stable lit pixels. For example, if (53, 48) is in $O_{(n,R)}$ and (48, 53) is in $O_{(R,n)}$, then 48 and 53 are a pair of stable lit pixels. Stable lit pixels are pixels with the stable DN value mapping relationship on the same position of the reference image and the calibrated images. As the distribution of the stable lit pixels is not always homogeneous on the DN value dimension, these points are only used to verify the effectiveness of RFM. The closer the fitted model is to the actual values of the stable lit pixels, the better the model is.

4. Results and discussion

4.1. *DMSP/OLS data calibration results*

Thirty-four DMSP/OLS data sets were calibrated using RFM. The calibration results (Figure 2) show that the calibration method in this study improved the comparability of DMSP/OLS data from 1992 to 2013. In Figure 2(c), the total number of lit pixels did not change after inter-calibration, because the RFM method can only change the DN value of the pixels but cannot change the lit pixels into non-lit pixels. We can find that after inter-calibration, the average DN values (Figure 2(d)) increase more smoothly than those in an un-calibrated image (Figure 2(b)). In most situations, inter-calibration reduced the discrepancies of the DN values between two satellites in the same year (Figure 2(d)). However, there are some abnormal fluctuations in the DN values from time-series data. The total number of lit pixels (Figure 2(e)) and the average DN values (Figure 2(f)) after intra-annual composition and series correction show that the discrepancies between the data were reduced. Overall, the fluctuations in time-series data were generally removed and the continuity and comparability of the time-series data were improved after the proposed calibration method.

To compare the performances of the RFM-based calibration and the traditional calibration, the same DMSP/OLS data sets were also calibrated using quadratic polynomials with the same reference satellite year (F162005) in Wuhan. Results from the two calibration methods are evaluated and compared based on the stable lit pixels. The mean squared error (MSE) of each fitted curve based on stable lit pixels was calculated based on the following equations:

$$M_{R_n} = \sum_{i=1}^{N_n} \left(D_{C_{(n,i)}} - I_{(n,i)} \right)^2 / N_n, \tag{5}$$

$$M_{Q_n} = \sum_{i=1}^{N_n} \left(Q_{C_{(n,i)}} - I_{(n,i)} \right)^2 / N_n, \tag{6}$$

where

M_{R_n} is the MSE of RFM,

M_{Q_n} is the MSE of quadratic polynomials,

$D_{C_{(n,i)}}$ is the inter-calibrated DN value using the RFM method,

$Q_{C_{(n,i)}}$ is the calibrated DN value using quadratic polynomials,

$I_{(n,i)}$ is the observed DN value of the extracted stable lit pixels in the nth data set,
N_n is the number of stable lit pixels, and
n represents the serial number of each data set.

We calculated the difference of mean square error (DMSE) between M_{R_n} and M_{Q_n} as a comparison as follows:

$$E_n = M_{Q_n} - M_{R_n}, \tag{7}$$

where $E_n$is the DMSE of the nth year. Positive DMSE means RFM is better than the quadratic polynomial. The larger the DMSE, the better the performance of the RFM compared with the quadratic polynomial.

Figure 3 shows the estimated RFM curves and the quadratic polynomials with all the lit pixels in each data set. From this figure, we can directly find that the RFM performs better than the quadratic polynomials. The RFM can fit the stable lit pixels well, especially for pixel DN values close to 63. Figure 4 shows the quantitative analysis results of each data set. The DMSE shows that RFM is better than the quadratic polynomials for 76% of the data set. Based on the above analysis, the RFM was chosen in this study to calibrate the night-time light data.

4.2. *Urban area expansion and construction policy analysis in Wuhan from 1992 to 2013*

DMSP/OLS night-time light data, which have more observation years, are feasible for long-term and macro-scale analysis. The weighted light urban areas in Wuhan in the DMSP/OLS data set from 1992 to 2013 were extracted based on the weighted light area, which was calculated by the sum of lit pixels multiplied by the normalized DN values (Equation 8). Pixels with DN values larger than 11 and less than or equal to 63 are considered in calculating the weighted light area to reduce the effects of dim lights (Ma et al. 2012). As shown in Figure 5, urban expansion was tremendous in Wuhan from 1992 to 2013. Wuhan has been the core city among the cities in Wuhan city circle; according to the city circle planning policy, the development of Wuhan was supposed to promote the development of the other cities in the city circle. Figure 5 shows that the development of the cities in Wuhan city circle had the same trend as that of Wuhan.

$$A = \sum S_i \times \left(d_i / \sum d_i\right), \ (d_i = 12, 13, 14 \ldots 63), \tag{8}$$

where
A is the weighted light area,
S_i is the pixel number of each DN value, and
d_i is the DN value.

The increment of weighted light area in the time-series data is shown in Figure 6. The increment value in each year was calculated based on the following equation:

$$I(n) = A(n) - A(n-1), \ n = 1993, 1994, 1995 \ldots 2013, \tag{9}$$

where
I is the increment value,
A is the weighted light area, and
n represents the year.

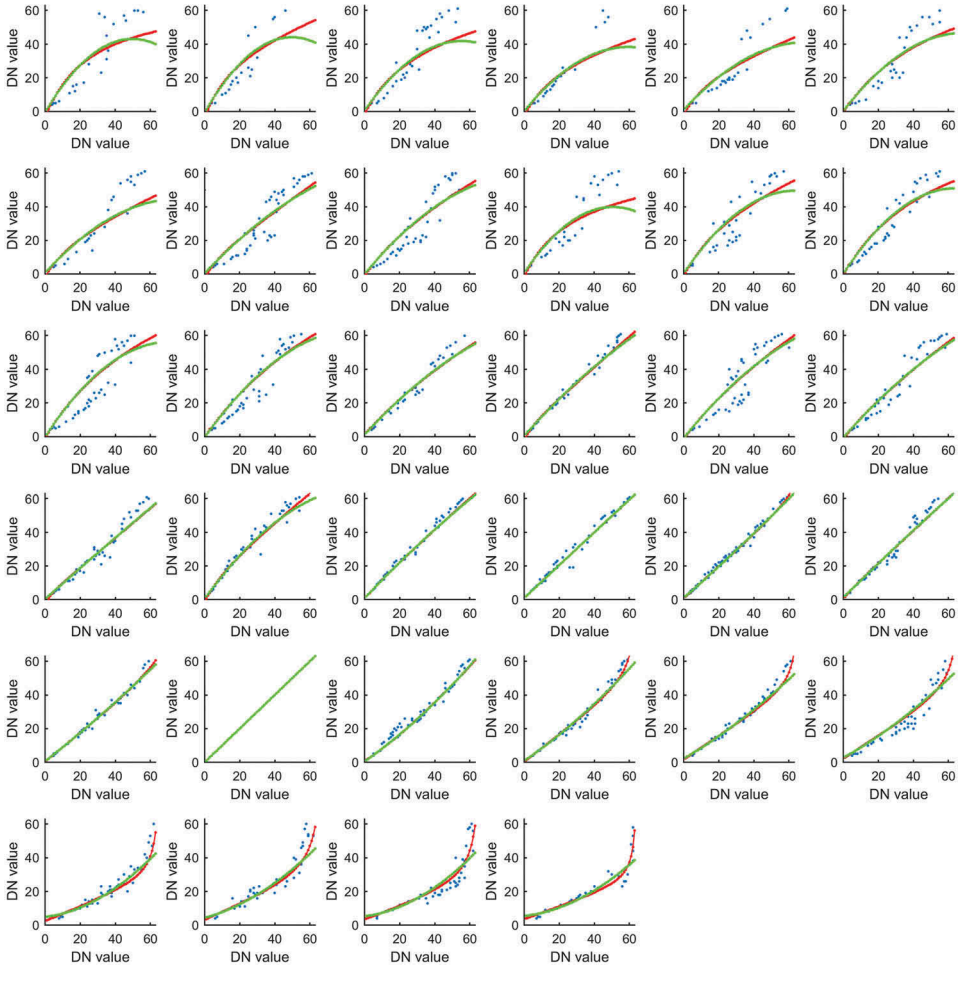

Figure 3. Fitted curves of RFM and the quadratic polynomials for the data sets. Each graph corresponds to one different data set as listed in Table 1. The blue points are the extracted stable lit pixels in each data set. The red lines are the RFM fitted curves with all the lit pixels and the green lines are the quadratic polynomials fitted curves with all the lit pixels in each data set.

According to Wuhan's construction policies from 1988 to 2010, there were four expansion stages in three Wuhan economic zones (Donghu New Technology Development Zone, Wuhan Economic and Technological Development Zone, and Wujiashan Economic Development Zone), including the start-up stage (1988–1993), the first expansion stage (2000–2001), the second expansion stage (2005–2007), and the third expansion stage (2010). Figure 6 shows five maximum values in five different years, and four of them reflect the four stages of expansion. It is also interesting to see that the maximum values in Figure 6 appear one year later than the end years of the expansion stages. This time lag is reasonable because the annual average data cannot reveal the constructions of buildings and roads that are finished and utilized in the end of the year.

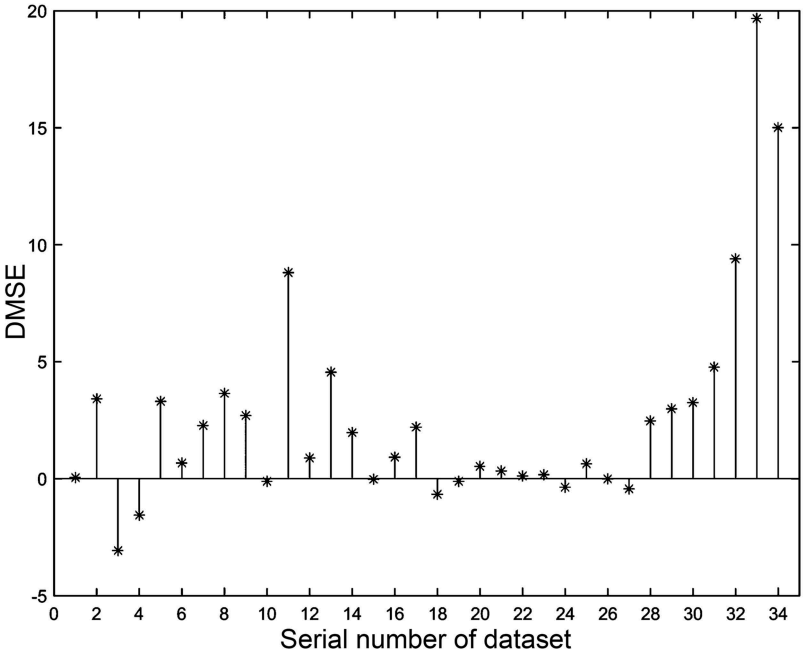

Figure 4. The scatter plot of DMSE in each data set.

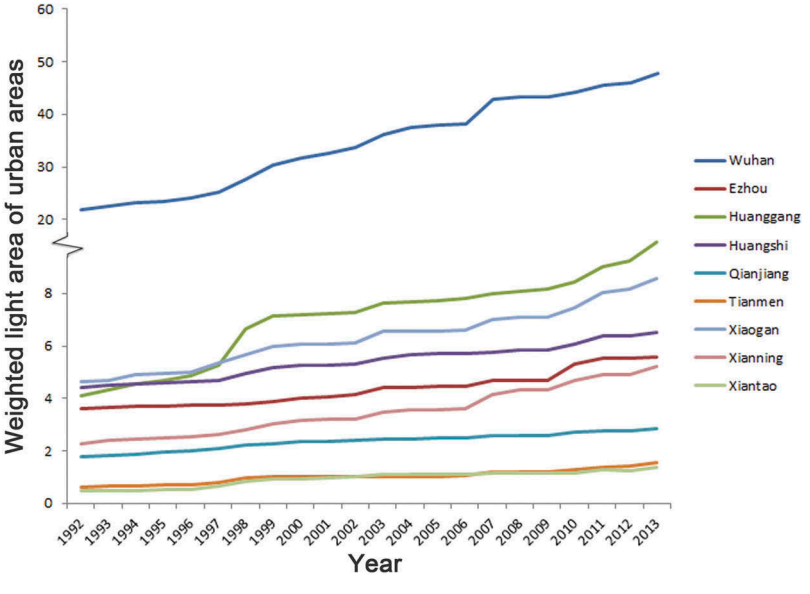

Figure 5. Comparative graph of the expansion of each of the cities in Wuhan city circle from 1992 to 2013.

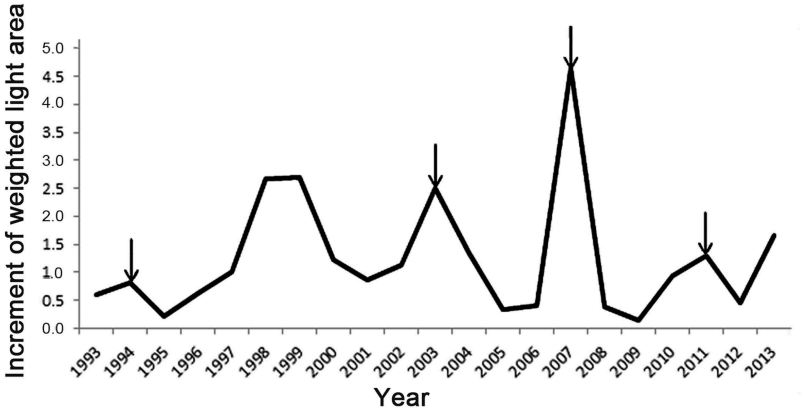

Figure 6. Increment of weighted light area per year in the time-series data in Wuhan. The arrows represent the expansion stages reflected in DMSP/OLS data.

4.3. *Socio-economic analysis in Wuhan and a comparative city Ordos*

The relationships between the weighted light area and socio-economic factors, GDP (X1), urban area (X2), electricity consumption (X3), population (X4), and population density (X5), were calculated through linear correlation analysis. The correlation coefficients (r, Equation 10) between the weighted light area and the socio-economic factors are shown in Figure 7. All the factors have a strong correlation with the weighted light area with a correlation coefficient (r) higher than 0.75. The results show that night-time light data have the highest correlation with population (X4).

$$r = \frac{\sum (x_i - \bar{x})(y_i - \bar{y})}{\sqrt{\sum (x_i - \bar{x})^2 \sum (y_i - \bar{y})^2}}, \tag{10}$$

where

r is the correlation coefficient,

x_i and y_i are the weighted light area and the socio-economic factor, respectively, and

$\bar{x}$ and $\bar{y}$ are the mean values of the weighted light area and the socio-economic factor, respectively.

We also performed linear regression analysis for all the five factors (X1, X2, X3, X4, and X5). Table 3 shows the results of unary and multiple linear regression analysis. It is identical to the correlation analysis results that the adjusted coefficient of determination (R^2, equation 11) of population (X4) is higher than that of any other factor in the unary linear regression. In the two-factor regression analysis, we can see that the values of R^2 of the combinations of urban area (X2) and other factors are always higher than those of the single factors (i.e. R^2 of XnX2 is higher than that of Xn and X2, n = 1, 3, 4, 5), and population (X4) has the same enhancement effect on the other factors. Thus, we can conclude that population and urban area are the enhancement factors in Wuhan. We can also find that some combinations containing population density (X5) resulted in a lower R^2 than that of the single factors.

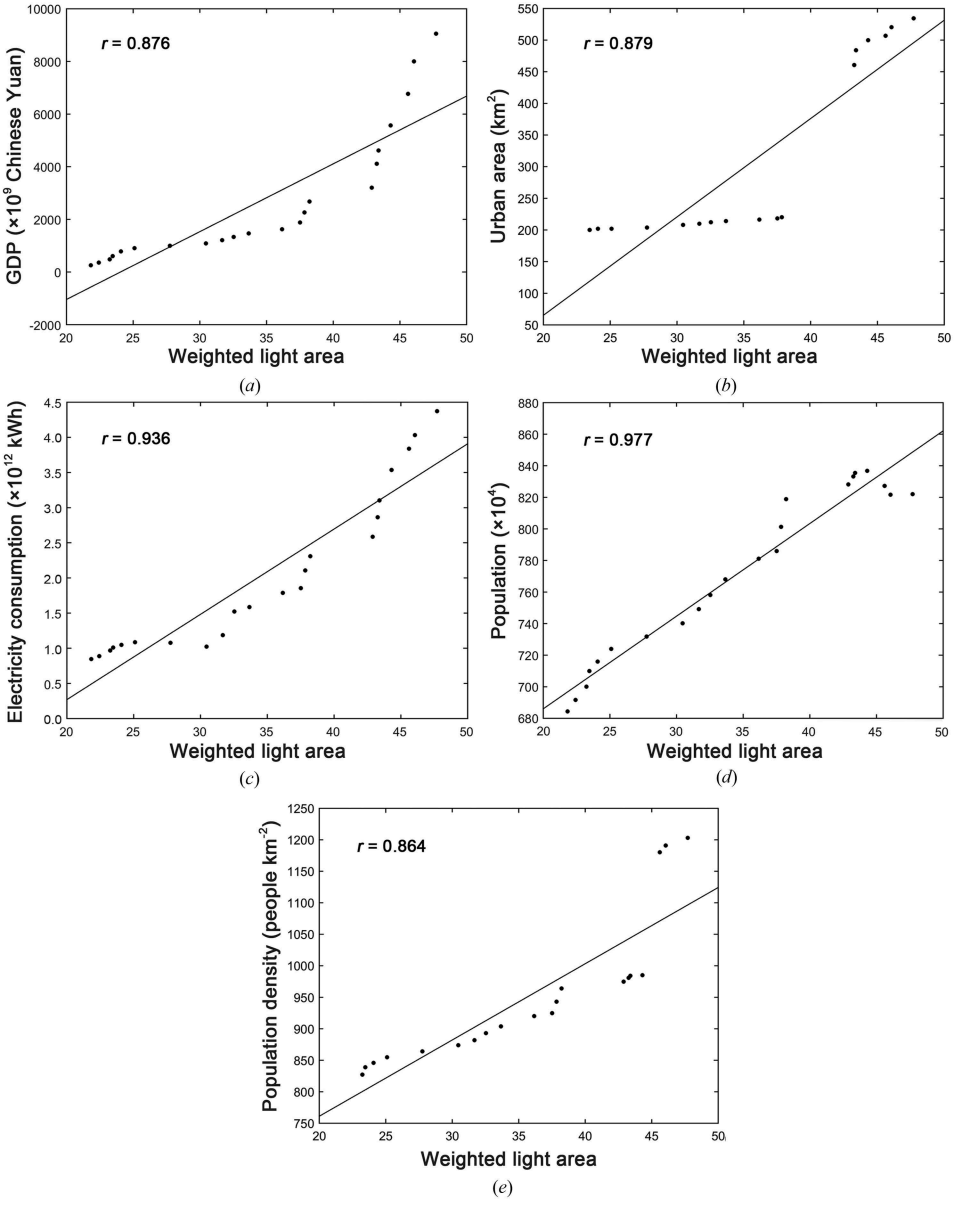

Figure 7. Linear correlation analysis results. (*a*) GDP versus weighted lighted area, (*b*) urban area versus weighted light area, (*c*) electricity consumption versus weighted light area, (*d*) population versus weighted lighted area, and (*e*) population density versus weighted light area. The points are the socio-economic factor values in different weighted light areas from 1992 to 2013. The lines are the regression curves.

$$R^2 = 1 - \left(\frac{m-1}{m-e}\right)\frac{\sum\left(Y_i - \widehat{Y}_i\right)^2}{\sum\left(Y_i - \overline{Y}_i\right)^2}, \tag{11}$$

Table 3. The R^2 of unary and multiple linear regression analysis in Wuhan.

One factor	R^2	Two factors	R^2
X1	0.775	X1X2	0.776
X2	0.757	X1X3	0.911
X3	0.870	X1X4	0.981
X4	0.951	X1X5	0.738
X5	0.733	X2X3	0.880
		X2X4	0.955
		X2X5	0.791
		X3X4	0.977
		X3X5	0.864
		X4X5	0.979

where

R^2 is the adjusted coefficient of determination,

Y_i is the observed value,

$\widehat{Y}_i$ is the estimated value,

$\overline{Y_i}$ is the mean value,

m is the number of observations, and

e is the number of regression coefficients.

To illustrate the significance of multiple linear regression analysis, the same analysis was performed for Ordos, a city in Inner Mongolia, China, as a comparative experiment. Table 4 shows the multiple linear regression result in Ordos. It shows that GDP (X1) has the highest R^2 among all the factors, urban area has the lowest R^2 among all the factors, and population density is the enhancement factor in Ordos.

There was a good linear relation between electricity consumption (X3) and weighted light area in Wuhan and Ordos, because electric lighting has a direct causal relationship with electricity consumption. By comparison, we find that population (X4) and weighted light area had the highest correlation (R^2 = 0.951) in Wuhan. Population in Wuhan has the highest R^2 because the increasing population has similar growth trends as the urban area. However, Wuhan has been developed around the Yangtze River, and there is an urban expansion limit that made the R^2 of the combination containing population density (X5) lower than that of single factors in the corresponding combinations. However, in Ordos, GDP (X1) and weighted light area have the highest correlation (R^2 = 0.908). Ordos is a typical resource-driven city in China. The exploitation of the resources resulted in the rapid growth of GDP and urban expansion, but there was no growth in population accordingly. Therefore, night-time light data in Ordos has a larger

Table 4. The R^2 of unary and multiple linear regression analysis in Ordos.

One factor	R^2	Two factors	R^2
X1	0.908	X1X2	0.907
X2	0.761	X1X3	0.904
X3	0.890	X1X4	0.899
X4	0.849	X1X5	0.914
X5	0.839	X2X3	0.881
		X2X4	0.863
		X2X5	0.874
		X3X4	0.890
		X3X5	0.928
		X4X5	0.880

correlation with GDP than population. Compared with analysing the relation between a single socio-economic factor and night-time light data, multiple linear regression analysis revealed more information about the city. The development driving forces of the cities could be reflected according to our research.

4.4. *Dynamic analysis between urban expansion and construction policy using NPP*

NPP/VIIRS data, which have a higher resolution than DMSP data, were employed for a more detailed study in the Wuhan City Administrative Region. The lit area was extracted through an optimal threshold (Milesi et al. 2003), which was selected through the correspondence between the lit area from the December 2014 and January 2015 NPP/VIIRS data and the urban area in Statistic Yearbook of Wuhan (Wuhan Bureau of Statistics 1992-2013). Through comparison between the lit area and the urban area in Wuhan, we used 24.72 as the threshold of lit area extraction. The extracted urban and urban change information are shown in Figure 8. The stable area (area that did not change in the different time phases), the expansion area, and the shrinkage area from January 2014 to August 2015 were all extracted by this method. By combining information on the construction policies, we extracted five typical change regions, including A) the Gusaoshu expressway (open to traffic on 28 April 2014), B) the Hanyang Binjiang Avenue (the second-stage project in 2015), C) the Yingwuzhou Yangtze River Bridge (open to traffic on 28 December 2014), D) the Lizhi Road (the first stage of reconstruction was completed at the end of 2014), and E) the Second Yangtze River Bridge of Wuhan (traffic control was cancelled from 22 July 2015).

The NPP/VIIRS night-time light data not only reflected the urban construction policy in the long term (blue rectangle in Figure 8), but also manifested the urban transport policy in the short term (green rectangle in Figure 8). The micro-scale human activities, e.g. those caused by traffic restriction on the Wuhan Yangtze River Bridge and the opening of new roads, can be revealed in the NPP/VIIRS night-time light data.

5. Conclusions

This article presented a new data calibration method for DMSP/OLS based on RFM. The proposed method achieved lower MSE than the conventional method (the quadratic polynomial model). The urban areas of Wuhan were extracted based on DMSP/OLS data after the calibration, and the extracted urban areas reflected the socio-economic activities and the construction policy. Correlation analysis was applied between the socio-economic data and the DMSP/OLS night-time light data from 1992 to 2013. Our results showed a strong correlation between the night-time light data and the socio-economic factors, especially for the population ($r = 0.977$). Multiple linear regression analysis showed that the R^2 of the combination results that contained the urban area and the population was higher than that of any other single factor in the corresponding combination result in Wuhan. A comparative experiment of multiple linear regression analysis was also carried out in Ordos, and the results show GDP has the highest R^2 among all the factors, and population density is the enhancement factor in Ordos. The comparative results indicated that the development driving forces of the cities could be reflected in multiple linear regression analysis of the socio-economic data and the night-time light data. A detailed study was carried out in Wuhan based on NPP/VIIRS night-time light data to illustrate the capability of revealing short-term construction policy.

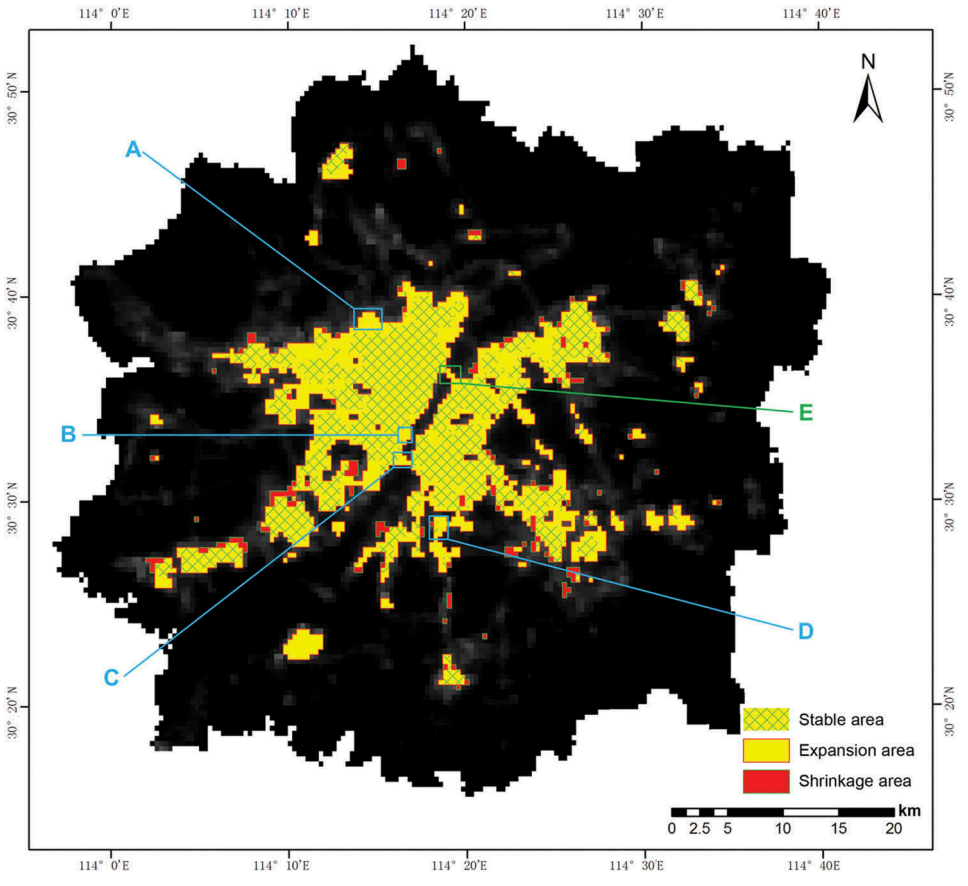

Figure 8. Changing results among different time phases from NPP/VIIRS data. a) Gusaoshu expressway, b) Hanyang Binjiang Avenue, c) Yingwuzhou Yangtze River Bridge, d) Lizhi Road, and e) Second Yangtze River Bridge of Wuhan. The green grid with yellow background covers the stable area (area that did not change in the different time phases), the yellow background covers the expansion area (area that increased in the next time phases), and the red background covered the shrinkage area (area that reduced in the next time phases) The NPP/VIIRS data were acquired in July 2015.

The results showed that high-resolution night-time light data can be used in monitoring micro-scale human activities caused by traffic restriction on the Wuhan Yangtze River Bridge and by the opening of new roads.

This research provides a case study in Wuhan and a comparative study in Ordos, which may not be representative of many other cities. Future research may focus on applying our methods to other major cities in different parts of the world, and evaluating whether our methods can be well generalized.

Acknowledgements

The authors are grateful to the editor Professor Warner and the three reviewers for their careful proofreading and insightful comments. This work was supported in part by National Natural Science Foundation of China (Grant Nos. 91538106 and 41501503). The authors would like to thank the NGDC/NOAA for providing the DMSP/OLS and NPP/VIIRS night-time light data, the

Wuhan Bureau of Statistics for the statistical data, the Wuhan Academy of Surveying and Mapping for the policy data and the information of expansion stages in three Wuhan economic zones.

Disclosure statement

No potential conflict of interest was reported by the authors.

Funding

This work was supported in part by National Natural Science Foundation of China (Grant Nos. 91538106 and 41501503).

References

Amaral, S., G. Câmara, A. M. V. Monteiro, J. A. Quintanilha, and C. D. Elvidge. 2005. "Estimating Population and Energy Consumption in Brazilian Amazonia Using DMSP Night-Time Satellite Data." *Computers, Environment and Urban Systems* 29: 179–195. doi:10.1016/j.compenvurbsys.2003.09.004.

Elvidge, C. D., K. E. Baugh, E. A. Kihn, H. W. Korehl, and E. R. Davis. 1997. "Mapping City Lights with Nighttime Data from the DMSP Operational Linescan System." *Photogrammetric Engineering & Remote Sensing* 63 (6): 727–734.

Elvidge, C. D., P. Cinzano, D. R. Pettit, J. Arvesen, P. Sutton, C. Small, R. Nemani, et al. 2007. "The Nightsat Mission Concept." *International Journal of Remote Sensing* 28 (12): 2645–2670. doi:10.1080/01431160600981525.

Elvidge, C. D., H. W. Kroehl, E. A. Kihn, K. E. Baugh, E. R. Davis, and W. M. Hao. 1995. "Algorithm for the Retrieval of Fire Pixels from DMSP Operational Linescan System Data." In *Global Biomass Burning*, edited by J. S. Levine, 73–85. Cambridge, Massachusetts: MIT Press.

Elvidge, C. D., D. Ziskin, K. E. Baugh, B. T. Tuttle, T. Ghosh, D. W. Pack, E. H. Erwin, and M. Zhizhin. 2009. "A Fifteen Year Record of Global Natural Gas Flaring Derived from Satellite Data." *Energies* 2: 595–622. doi:10.3390/en20300595.

Imhoff, M. L., W. T. Lawrence, D. C. Stutzer, and C. D. Elvidge. 1997. "A Technique for Using Composite DMSP/OLS "City Lights" Satellite Data to Map Urban Area." *Remote Sensing of Environment* 61: 361–370. doi:10.1016/s0034-4257(97)00046-1.

Johnson, D. B., P. Flament, and R. L. Bernstein. 1994. "High-Resolution Satellite Imagery for Mesoscale Meteorological Studies." *Bulletin of the American Meteorological Society* 75 (1): 5–33. doi:10.1175/1520-0477(1994)075<0005:HRSIFM>2.0.CO;2.

Lee, T. E., S. D. Miller, F. J. Turk, C. Schueler, R. Julian, S. Deyo, P. Dills, and S. Wang. 2006. "The NPOESS VIIRS Day/Night Visible Sensor." *Bulletin of the American Meteorological Society* 87 (2): 191–199. doi:10.1175/BAMS-87-2-191.

Levin, N., and Y. Duke. 2012. "High Spatial Resolution Night-Time Light Images for Demographic and Socio-Economic Studies." *Remote Sensing of Environment* 119: 1–10. doi:10.1016/j.rse.2011.12.005.

Li, B. 2008. "Urban Development Policies of China and the Influence to Chinese Urbanization." *(In Chinese) Urban Studies* 14 (2): 26–37. doi:10.3969/j.issn.1006-3862.2008.02.005.

Li, X., and D. Li. 2014. "Can Night-Time Light Images Play a Role in Evaluating the Syrian Crisis." *International Journal of Remote Sensing* 35 (18): 6648–6661. doi:10.1080/01431161.2014.971469.

Li, X., R. Zhang, C. Huang, and D. Li. 2015. "Detecting 2014 Northern Iraq Insurgency Using Night-Time Light Imagery." *International Journal of Remote Sensing* 36 (13): 3446–3458. doi:10.1080/01431161.2015.1059968.

Liu, Z. F., C. Y. He, Q. F. Zhang, Q. X. Huang, and Y. Yang. 2012. "Extracting the Dynamics of Urban Expansion in China Using DMSP-OLS Nighttime Light Data from 1992 to 2008." *Landscape and Urban Planning* 106: 62–72. doi:10.1016/j.landurbplan.2012.02.013.

Ma, T., C. Zhou, T. Pei, S. Haynie, and J. Fan. 2012. "Quantitative Estimation of Urbanization Dynamics Using Time Series of DMSP/OLS Nighttime Light Data: A Comparative Case Study from China's Cities." *Remote Sensing of Environment* 124: 99–107. doi:10.1016/j.rse.2012.04.018.

Milesi, C., C. D. Elvidge, R. R. Nemani, and S. W. Running. 2003. "Assessing the Impact of Urban Land Development on Net Primary Productivity in the Southeastern United States." *Remote Sensing of Environment* 86: 401–410. doi:10.1016/S0034-4257(03)00081-6.

Mills, S., S. Weiss, and C. Liang. 2013. "VIIRS Day/Night Band (DNB) Stray Light Characterization and Correction." *Proceedings of SPIE* 8866 (1P). doi:10.1117/12.2023107.

Ou, J., X. Liu, X. Li, M. Li, and W. Li. 2015. "Evaluation of NPP-VIIRS Nighttime Light Data for Mapping Global Fossil Fuel Combustion CO2 Emissions: A Comparison with DMSP-OLS Nighttime Light Data." *PLoS One* 10 (9): e0138310. doi:10.1371/journal.pone.0138310.

Press, W. H., S. A. Teukolsky, W. T. Vetterling, and B. P. Flannery, (2007). "Rational Function Interpolation and Extrapolation". Chap. 3.4. In *Numerical Recipes: The Art of Scientific Computing*. 3rd. New York, NY: Cambridge University Press.

Shi, K., C. Huang, B. Yu, B. Yin, Y. Huang, and J. Wu. 2014a. "Evaluation of NPP-VIIRS Night-Time Light Composite Data for Extracting Built-Up Urban Areas." *Remote Sensing Letters* 5 (4): 358–366. doi:10.1080/2150704X.2014.905728.

Shi, K., B. Yu, Y. Huang, Y. Hu, B. Yin, Z. Chen, L. Chen, and J. Wu. 2014b. "Evaluating the Ability of NPP-VIIRS Nighttime Light Data to Estimate the Gross Domestic Product and the Electric Power Consumption of China at Multiple Scales: A Comparison with DMSP-OLS Data." *Remote Sensing* 6: 1705–1724. doi:10.3390/rs6021705.

Small, C., F. Pozzi, and C. D. Elvidge. 2005. "Spatial Analysis of Global Urban Extent from DMSP-OLS Night Lights." *Remote Sensing of Environment* 96: 277–291. doi:10.1016/j.rse.2005.02.002.

Snyder, J. P. 1987. *Map Projections-A Working Manual*. Washington, DC: U.S. Government Printing Office.

Sutton, P., D. Roberts, C. Elvidge, and K. Baugh. 2001. "Census from Heaven: An Estimate of the Global Human Population Using Night-Time Satellite Imagery." *International Journal of Remote Sensing* 22 (16): 3061–3076. doi:10.1080/01431160010007015.

Wuhan Bureau of Statistics. 1992-2013. *Statistic Yearbook of Wuhan*. Beijing: China Statistics Press.

Xia, L., K. Mao, Z. Sun, Y. Ma, and F. Zhao. 2014. "Method for Detecting Cloud at Night from VIIRS Data Based on DNB." *Remote Sensing for Land & Resources* 26 (3): 74–79. doi:10.6046/gtzyyg.2014.03.12.

Zhang, Q., and K. C. Seto. 2011. "Mapping Urbanization Dynamics at Regional and Global Scales Using Multi-Temporal DMSP/OLS Nighttime Light Data." *Remote Sensing of Environment* 115: 2320–2329. doi:10.1016/j.rse.2011.04.032.

Zhao, N., Y. Zhou, and E. L. Samson. 2015. "Correcting Incompatible DN Values and Geometric Errors in Nighttime Lights Time-Series Images." *IEEE Transactions on Geoscience and Remote Sensing* 53 (4): 2039–2049. doi:10.1109/TGRS.2014.2352598.

Zhou, Y., S. J. Smith, C. D. Elvidge, K. Zhao, A. Thomson, and M. Imhoff. 2014. "A Cluster-Based Method to Map Urban Area from DMSP/OLS Nightlights." *Remote Sensing of Environment* 147: 173–185. doi:10.1016/j.rse.2014.03.004.

Zhu, Z., Y. Fu, C. E. Woodcock, P. Olofsson, J. E. Vogelmann, C. Holden, M. Wang, S. Dai, and Y. Yu. 2016. "Including Land Cover Change in Analysis of Greenness Trends Using All Available Landsat 5, 7, and 8 Images: A Case Study from Guangzhou, China (2000–2014)." *Remote Sensing of Environment* 185: 243–257. doi:10.1016/j.rse.2016.03.036.